



The human mediodorsal thalamus: Organization, connectivity, and function

Kaixin Li^{a,b,c,1}, Lingzhong Fan^{b,c,d,e,1}, Yue Cui^{b,c,e}, Xuehu Wei^f, Yini He^g, Jiyue Yang^{b,c,e},
Yuheng Lu^{b,c,e}, Wen Li^{b,c,e}, Weiyang Shi^{b,c,e}, Long Cao^{b,c,h}, Luqi Cheng^{b,c,i}, Ang Li^j, Bo You^{a,*},
Tianzi Jiang^{b,c,d,e,h,k,*}

^a School of Mechanical and Power Engineering, Harbin University of Science and Technology, Harbin 150080, China

^b Brainnetome Center, Institute of Automation, Chinese Academy of Sciences, Beijing 100190, China

^c National Laboratory of Pattern Recognition, Institute of Automation, Chinese Academy of Sciences Beijing 100190, China

^d CAS Center for Excellence in Brain Science and Intelligence Technology, Institute of Automation, Chinese Academy of Sciences, Beijing 100190, China

^e School of Artificial Intelligence University of Chinese Academy of Sciences, Beijing 100190, China

^f Department of Neuropsychology, Max Planck Institute for Human Cognitive and Brain Sciences, Leipzig, Germany

^g State Key Laboratory of Cognitive Neuroscience and Learning, Beijing Normal University, Beijing, China

^h Key Laboratory for NeuroInformation of Ministry of Education, School of Life Science and Technology, University of Electronic Science and Technology of China, Chengdu 610054, China

ⁱ School of Life and Environmental Sciences, Guilin University of Electronic Technology, Guilin 541004, China

^j State Key Laboratory of Brain and Cognitive Science, Institute of Biophysics, Chinese Academy of Sciences, Beijing 100101, China

^k The Queensland Brain Institute, University of Queensland, Brisbane, QLD 4072, Australia

ARTICLE INFO

Keywords:

Mediodorsal thalamic nucleus
Parcellation
Anatomical organization
Functional connectivity
Cognitive functions

ABSTRACT

The human mediodorsal thalamic nucleus (MD) is crucial for higher cognitive functions, while the fine anatomical organization of the MD and the function of each subregion remain elusive. In this study, using high-resolution data provided by the Human Connectome Project, an anatomical connectivity-based method was adopted to unveil the topographic organization of the MD. Four fine-grained subregions were identified in each hemisphere, including the medial (MDm), central (MDc), dorsal (MDd), and lateral (MDl), which recapitulated previous cytoarchitectonic boundaries from histological studies. The subsequent connectivity analysis of the subregions also demonstrated distinct anatomical and functional connectivity patterns, especially with the prefrontal cortex. To further evaluate the function of MD subregions, partial least squares analysis was performed to examine the relationship between different prefrontal-subregion connectivity and behavioral measures in 1012 subjects. The results showed subregion-specific involvement in a range of cognitive functions. Specifically, the MDm predominantly subserved emotional-cognition domains, while the MDl was involved in multiple cognitive functions especially cognitive flexibility and inhibition. The MDc and MDd were correlated with fluid intelligence, processing speed, and emotional cognition. In conclusion, our work provides new insights into the anatomical and functional organization of the MD and highlights the various roles of the prefrontal-thalamic circuitry in human cognition.

1. Introduction

The mediodorsal thalamic nucleus (MD), a higher-order relay nucleus, is involved in regulating cortical networks (Guillery, 1995; Sherman, 2007). As a key structure related to many neurological and psychiatric diseases (Golden et al., 2016; Mitchell and Chakraborty, 2013), the MD was thought to be a potential target for deep brain stimulation (DBS) treatment for resistant schizophrenia (Mavridis, 2014). Anatomical evidence shows that the MD plays a crucial role in multiple cognitive functions (Mitchell, 2015; Mitchell and

Chakraborty, 2013) including attention, planning, abstract thinking, emotion, and working memory through its extensive connections with the prefrontal cortex (Haber and McFarland, 2001; Oyoshi et al., 1996). However, the detailed structural organization of the MD and the rules that explicate the relationship between its subregions and human behaviors remain poorly understood.

The subregions of the MD have been defined primarily by studying its anatomical microstructure (Jones, 2012; Morel et al., 1997; Ray and Price, 1993). In nonhuman primates, the MD is generally subdivided into 3 parts based on cytoarchitecture, namely the magnocellular mid-

* Corresponding authors.

E-mail addresses: youbu@hrbust.edu.cn (B. You), jiangtz@nlpr.ia.ac.cn (T. Jiang).

¹ Kaixin Li and Lingzhong Fan Co-first author.

dle, parvocellular central, and multiform or paralamellar lateral parts (Mitchell and Chakraborty, 2013; Ray and Price, 1992). In the human brain, Morel's histological atlas of the thalamus identified three distinct subdivisions in the MD (Morel et al., 1997). Another human histological atlas described a dense cellular caudodorsal region of the MD (Ding et al., 2016). Compared to the traditional histological studies, the subregions could also be discerned by the main structural connections using in vivo diffusion magnetic resonance imaging (dMRI) (Klein et al., 2010; Phillips et al., 2019). Furthermore, by calculating the connectivity pattern of the subregion, the connectivity between the subregion and a set of target regions can be quantitatively characterized (Cheng et al., 2018; Zhang et al., 2017; Zhuo et al., 2016). Hence, a connectivity-based approach may more accurately reflect the structural topography of the MD.

Moreover, a large number of studies on animal experiments and injury studies have confirmed an important role of the MD in cognition from a functional perspective. Animal models have emphasized that, because of its robust structural interconnections with other brain areas, the MD is essential in integrating various affective behaviors and in cognitive processing (for review, (Georgescu et al., 2020; Pergola et al., 2018)). Previous lesion studies on human patients revealed that neurological and psychiatric diseases such as schizophrenia are related to injuries of different parts of the MD and that the interaction between the damaged part and the cortex may lead to different aspects of cognitive impairment, such as the disruption of executive function and learning deficits (Alelú-Paz and Giménez-Amaya, 2008; Mitchell et al., 2007; Ouhaz et al., 2018; Pergola et al., 2013; Victor, 1989). In healthy humans, few neuroimaging studies have investigated the functions of the MD. Precise subregions can provide cognitive insights about a brain region in that the interactions between spatially distributed brain regions are taken into account, which might be the cause of complex behaviors (Zimmermann et al., 2018). Therefore, it is necessary to see whether the connections of different subregions relate to different cognitive functions.

In this study, we aimed to identify and characterize the subregions of the human MD and explore the underlying behaviors of each MD subregion using in vivo MRI data. We first obtained a robust parcellation of the human MD based on its whole-brain anatomical connectivity conducted on a representative high-resolution dataset from the Human Connectome Project (HCP). Then we explored the anatomical and functional connectivity of each subregion with the rest of the brain. Finally, a partial least squares correlation (PLSC) model was used to explore the relationships between each subregion's functional connectivity and human behavioral measures. The goal of this study was to provide a comprehensive description of the MD, which could benefit brain interventions and treatment in clinical situations.

2. Materials and methods

2.1. Subjects

We used 40 unrelated subjects (age: 22–35, 20 male) from the HCP database for a connectivity-based segmentation of the MD. Detailed demographic information about these subjects was described previously (Fan et al., 2016). To characterize the connectivity pattern of each subregion and its relationship with behaviors, the data from 1012 healthy young adults (age: 22–35; 469 males) with both diffusion and functional imaging data were extracted from the S1200 subjects release of the WU-Minn HCP Consortium (Van Essen et al., 2013). The data for the subjects were collected using a Siemens 3T scanner (Siemens, Erlangen, Germany) with a 32-channel head coil. The scanning procedures and parameters are described in detail in Van Essen et al. (2013) and also provided in the supplementary materials. In this study, 59 behavioral measures (Supplementary Table S1) were used to explore the brain-behavior relationships (Tian and Zalesky, 2018). A detailed description of the measures is available at

<https://wiki.humanconnectome.org/display/PublicData/HCP+Data+Dictionary+Updated+for+the+1200+Subject+Release>

2.2. Data preprocessing

Diffusion MRI: The HCP diffusion images with 1.25 mm isotropic spatial resolution were preprocessed by the HCP diffusion preprocessing pipeline using the FMRIB diffusion toolbox (FSL 5.0; <http://www.fmrib.ox.ac.uk/fsl>). The main steps are as follows: normalization of b0 image intensity across runs and correction for echo-planar imaging (EPI) susceptibility, eddy-current-induced distortions, gradient-nonlinearities, and subject motion. The probability distributions of the fiber orientations were estimated using FSL's BEDPOSTX algorithm (Behrens et al., 2007). Next, skull-stripped T1-weighted images for each subject were co-registered to the subject's b0 images using FSL's FLIRT algorithm. Then we derived linear and nonlinear transformations between the T1 image and the Montreal Neurological Institute (MNI) structural template. Based on these, we derived (forward and inverse) transformations between the diffusion space and the MNI space, which were then used to transform the seed masks into the diffusion space for each subject.

Resting-state fMRI: There were four 15-minute rs-fMRI scans for each subject. All the images were visually inspected and minimally preprocessed by HCP personnel before release (e.g., distortion corrected, coregistered, and warped to MNI and CIFTI grayordinate templates; see Glasser et al. (2013) for details). Whole-brain connectivity analyses were performed using rs-fMRI data in CIFTI grayordinate space, which represents the cortex using surface meshes (32k vertices per surface) and the subcortex using 3D MNI coordinates (2 mm isotropic spatial resolution). The ROI time-series were extracted from the unsmoothed rs-fMRI data in the MNI space. The rs-fMRI data were bandpass filtered (0.1 - 0.01 Hz). To spatially smooth the data, a 4 mm FWHM Gaussian kernel was applied only to the cortical surface using Connectome Workbench version 1.2.4 (Marcus et al., 2011).

2.3. Definition of ROI

Accurate delineation of the MD boundaries is crucial but challenging. In the present study, we identified individual MD boundaries by mapping a directionally-encoded color (DEC) map of the track-density imaging (TDI). Specifically, for each of the 40 subjects, we mapped the TDI of their data to gain a high spatial resolution of the white matter image using MRtrix3.0 (Calamante et al., 2010). The TDI image for each individual was then calculated at an isotropic spatial resolution of 0.5 mm and represented as a directionally-encoded color (DEC) map. The RGB-colored TDI map facilitated the in vivo delineation of the MD based on high anatomical contrast. We manually delineated the boundaries of the MD based on the DEC maps, which could define the voxels over which the orientations changed (Fan et al., 2011). We warped the individual DEC and edges maps into MNI standard space and acquired the group-averaged map at >70% probability which was shown in Supplementary Fig. S1. Concerning Morel thalamus atlas (Morel et al., 1997), we experimented with different thresholds, so that the group averaged map could optimally match the MD nucleus in the standard space. The highest coincidence map was obtained when the probability value was 70% and the final boundary of the MD was then identified.

2.4. Connectivity-based parcellation of the MD

The parcellation scheme is similar to our previous work (Supplementary Fig. S2) as described in (Cheng et al., 2021; Fan et al., 2016). First, we transformed the group level ROI into native DTI space and applied probabilistic tractography for each individual by sampling 5000 streamline fibers for each voxel in the seed region to estimate its whole-brain connectivity profile. After using a small threshold to reduce the false positives, we down-sampled the images to 5 mm isotropic resolution to

facilitate data storage (Johansen-Berg et al., 2004). Based on the correlations in the connectivity profile, we calculated the correlation matrix, which expresses the cross-correlations between each pair of voxels in the seed region (Johansen-Berg et al., 2004). Then, we applied spectral clustering to the similarity matrix, which automatically subdivided all the voxels in the seed mask into multiple subgroups (Baldassano et al., 2015), setting the number of potential clusters to range from 2 to 8. To get the most accurate and consistent parcellation map, we used some indicators to assist in the selection. The optimal cluster number was determined by the hierarchical index (HI) and topological distance (TpD). The HI was used to measure the hierarchical structure between different partition categories and partition modes (Tungaraza et al., 2015). An HI value closer to 1 indicates a more robust hierarchical structure among the partition modes. TpD was used to quantify the similarity in the topological arrangement of putatively homologous areas across hemispheres (Fan et al., 2016). The parcellation result for each subject was then mapped into MNI standard space, and a maximum probability map (MPM) was calculated as the final result, which considered the inter-individual differences in the MD parcellation (Caspers et al., 2008). The final subregions masks were generated by thresholding above 50% (i.e., 20 subjects) on the group-overlapped probability maps.

2.5. Comparisons of the MD parcellation with the Allen adult human atlas

The Allen Institute's anatomical reference atlas illustrates the adult human brain (cadaver specimens from a 34-year-old female), using modified Brodmann or gyral annotation (Ding et al., 2016). The ex-vivo dMRI data from this donor was acquired with a 3T scanner at 900-micron resolution (<http://atlas.brain-map.org/>). We utilized the same parcellation scheme and obtained a connectivity-based parcellation of the MD. We then compared the patterns between histological maps and the parcellations of the MD obtained using dMRI.

2.6. Mapping anatomical connectivity patterns

To estimate the connectivity pattern of the MD subregions, probabilistic fiber tracking was applied by sampling 10,000 streamline fibers per voxel (starting from the seed voxels in the MD subregions) for each of the 1012 subjects. The connectivity maps were first normalized by the size of the seed region and the total number of streamlines (i.e. 10,000) to generate the relative tracing strength from the seed to the rest of the brain (Xia et al., 2017; Zhang et al., 2017). Then a threshold of 0.38 was used to remove the noise effects of fiber tracking (Zhuo et al., 2016). For each subregion, the fiber tracts were binarized and transformed into MNI standard space. The resulting individual tractograms were averaged to generate a probability fiber map for each MD subregion. The map was then thresholded at 50% to generate the group-level whole-brain anatomical connectivity pattern for the given subregion. To obtain the fiber projection for each subregion, we also calculated the maximum probability map based on the fiber tracts (Zhang et al., 2017), in which the classification of each voxel in the combined connection mask was mainly based on the MD subregion with the highest connectivity.

To obtain a quantitative comparison for the anatomical connectivity of each MD subregion, the target ROI for each individual was derived from the Brainnetome Atlas for each hemisphere to estimate the anatomical connectivity. The Brainnetome Atlas is a fine-grained anatomical connectivity-based atlas containing 210 cortical and 36 subcortical subregions (Fan et al., 2016). The method for calculating the connectivity probabilities between a MD subregion and a target ROI has been described previously. (Xia et al., 2017; Zhuo et al., 2016). A univariate ANOVA was used to determine whether there was a specific connection difference between each subregion of the MD and the ipsilateral target region; *p* values were calculated with family-wise error (FWE) correction for multiple comparisons. These statistical analyses were performed

using Matlab version 2017. The connectivity maps along with the results of the quantitative analysis and previous studies indicated that the connectivity differences for each subregion were mainly concentrated in the prefrontal lobe, so we focused on 28 prefrontal subregions from the Brainnetome Atlas to investigate their cortical anatomical connectivity fingerprints. A connection probability value was averaged for each seed–target combination across all the subjects. To better delineate these target relationships, we normalized the connection strength of all the subregions with one target summing to 1.

2.7. Mapping resting-state functional connectivity patterns of the MD subregion

The MD subregional functional connectivity (FC) patterns were calculated by the correlation between the average time series for the MD subregions and the time series for each cortical surface vertex and subcortical voxel in 32k CIFTI grayordinate space (i.e., 91,282 total correlations) using the Connectome Workbench (Ely et al., 2019). The results from the four rs-fMRI runs for each subject were converted to *z* values using Fisher's *z* transformation and averaged to get subject-level connectivity maps. A random-effects one-sample *t*-test was used to determine the regions that had significant correlations with the MD subregion. Group-level connectivity statistics were corrected for FWE with a statistical significance of $p < 0.05$ and the extended threshold of the cluster size of the conjunction set at 50.

Using a method that corresponds to the quantitative analysis of anatomical connections, we did a similar analysis in terms of function connections. We mapped the functional connectivity patterns between each MD subregion and Yeo's seven intrinsic networks (Yeo et al., 2011) and also mapped the functional connectivity patterns between each MD subregion and the ipsilateral prefrontal subregions (Xia et al., 2017). A one-sample *t*-test was used to calculate the connection strength on the group level using a corrected (FWE $p < 0.05$) connection strength. Univariate ANOVAs and pairwise comparisons were performed to identify the specific differences between each pair of MD subregional connection probabilities with the target areas.

2.8. Correlation analysis between MD-prefrontal functional connectivity and cognitive measures

We used PLSC to analyze the relationship between the functional connectivity of the MD subregions and both the prefrontal lobe and the behavioral measures (behavioral PLS correlation, <http://www.rotman-baycrest.on.ca/pls>) (McIntosh et al., 1996; McIntosh and Lobaugh, 2004; Mišić et al., 2016). We used this method to identify pairs of latent variables (LVs) that correspond to brain activity and behavioral variables with maximal covariance. For each subject, the MD-prefrontal functional connectivity (FC) was calculated as the correlation between the average time series for each MD subregion and the average time series for each prefrontal region (58 regions in both groups) according to the Brainnetome Atlas (Fan et al., 2016). Then the *r* values were converted to *z* values using Fisher's *z* transformation. For each MD subregion, the brain matrix was the number of subjects multiplied by the number of connections (1012×58). Confounds included age, sex, and mean frame-wise displacement were regressed from Fisher's *z*-transformed FC before the PLS, and residuals were used for analysis. The behavioral matrix was the number of subjects multiplied by the number of behavioral measures (1012×59). The 59 behavioral measures tapped the functional domains known to be subserved by the MD.

The brain and behavior matrix were *z* scored and then cross-correlated to start the PLS. A singular value decomposition was employed to decompose the brain-behavior matrix into corresponding loadings. By projecting the brain and behavioral matrices onto their respective loadings, the LVs were obtained, providing an optimal depiction of the brain-behavior commonality and intra-individual characteristics. The significance of the LVs was evaluated by permutation tests using

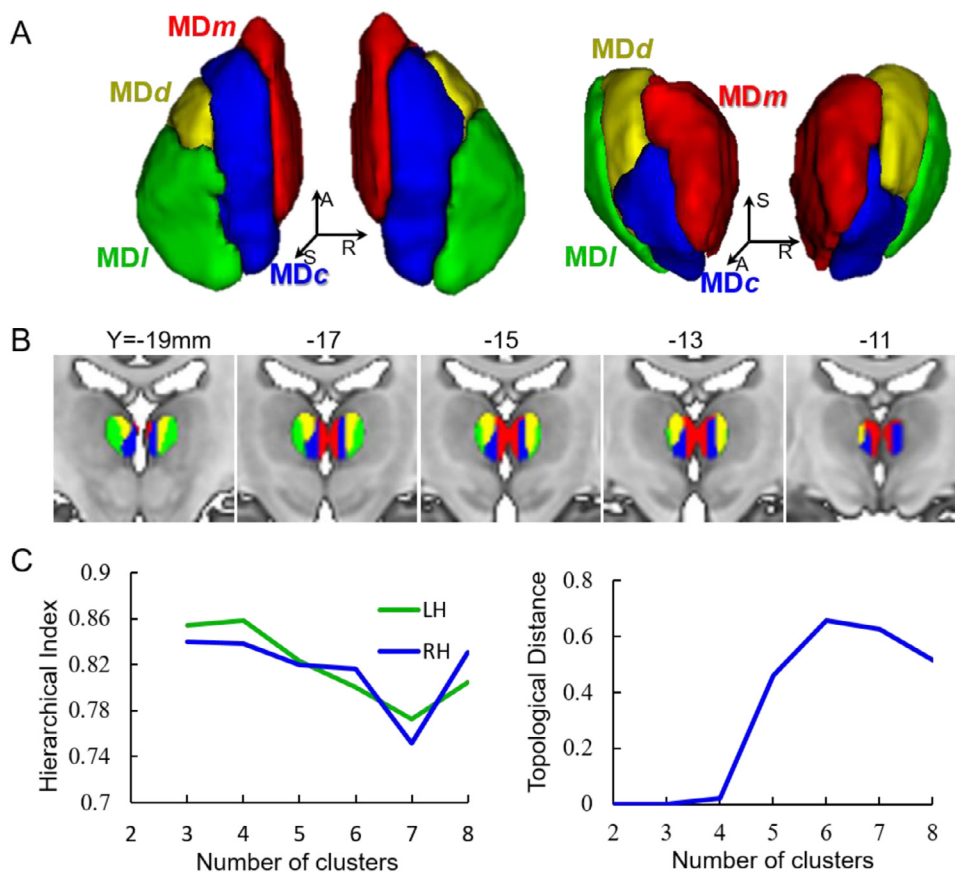


Fig. 1. Parcellation of the MD thalamus based on anatomical connectivity profiles. The MD was divided into four subregions: middle (MDm), central (MDC), dorsal (MDd), and lateral (MDl). (A) Three-dimensional model of the subregions. (B) Coronal MRI view of the subregions. (C) Hierarchical index and topological distance of the MD parcellation with cluster numbers from 2 to 8. The four-cluster parcellation of the MD showed a high hierarchical index and low topological distance. LH: Left hemisphere; RH: Right hemisphere.

1000 permutations, each comprising a row-shuffled brain matrix and an unchanged behavioral matrix. The significant LVs were identified using p values, which were computed as the probabilities that the permuted singular values exceeded the initial singular values. For each significant LV, the reliability of the contribution of each functional connection to the brain-behavior association was assessed as the ratio of its loading to its bootstrap-estimated standard error, called the bootstrap ratio. The standard errors were estimated through 3000 bootstrap samples, which were created by selecting subjects with replacement. Since the bootstrap ratio approximates to a z score and a high absolute value indicates that the FC has a large effect and is stable regardless of sample selection, the set threshold can identify FCs of significant reliability (e.g., a threshold of 2 corresponds to the 95th percentile). An FC with a high positive bootstrap ratio indicates a positive contribution to the brain-behavior association, whereas an FC with a high negative bootstrap ratio indicates a negative contribution to the brain-behavior relationship. We also used a bootstrap method to construct the significance and confidence intervals for the correlation between the brain and behavior.

3. Results

3.1. Subregions of the MD

We varied the number of subregions in the human MD from 2 to 8 based on spectral clustering of the connectivity patterns between the MD voxels. Then, we used the TpD across the hemispheres and the HI to determine the optimum number of subregions in the MD. As shown in Fig. 1C, both TpD and HI indicated 4 to be the most robust segmentation, in that the clusters were compact with a consistent principal spatial arrangement across the hemispheres. Therefore, we identified four subregions: the MDm (medial), MDC (central), MDd (dorsal), and MDl (lateral). The group-level segmentation of the MD was visualized using

a 3D model (Fig. 1A) and coronal MRI (Fig. 1B). As shown in Fig. 1C the four-subregion parcellation of the MD had the most stable hierarchy and topological distance. The volume of MD is consistent with the description in the previous article (Byrne et al., 2002; Liu et al., 2020; Su et al., 2019). The average whole volume of each subregion was the MDm: 174/180 mm³, MDC: 203/207 mm³, MDd: 186/204 mm³, and MDl: 191/167 mm³, for left/right, respectively (Supplementary Fig. S3).

The connectivity-based parcellation showed patterns that were similar to Allen's histological subdivisions. The MD sub-regions on a slice of Allen's histological map and the DTI data are shown in Supplementary Fig. S4.

3.2. Anatomical connectivity patterns of the MD subregions

In the current study, the connectivity profiles for each subregion of the MD were identified by performing diffusion probabilistic tractography on individual HCP participants. The anatomical connectivity pattern for each left and right MD subregion are illustrated in Fig. 2 and Supplementary Fig. S5. Each pattern indicates that the population probability of a voxel belonging to the pathway for each sub-region was >50%. Fig. 2 shows that the subregions tended to connect to the prefrontal cortex. In brief, the MDm was primarily connected to the medial orbitofrontal cortex. The MDC was anatomically connected with the orbitofrontal cortex. The MDd was connected to most of the ventrolateral prefrontal cortex area. The MDl had many projections to the prefrontal and anterior cingulum cortex.

To show the diversity of the four sub-regions in the connection mode, anatomical connectivity fingerprints for the four MD subregions (Fig. 3, Supplementary Fig. S6) were generated by mapping the connectivity profiles to the prefrontal subregions of the Brainnetome Atlas (Fan et al., 2016). As shown in Fig. 3, the MDm had greater connectivity with the Brodmann area (BA) 13 of the orbitofrontal cortex than the other sub-

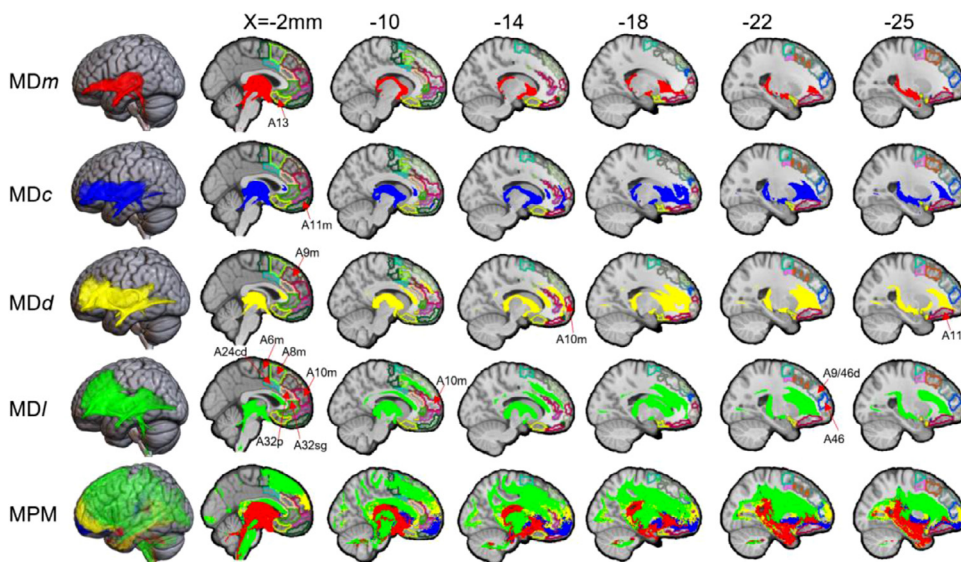


Fig. 2. Connectivity patterns and maximum probability tractograms (MPM) of the left MD, MDm (red), MDc (blue), MDd (yellow), and MDl (green). Probabilistic tractography was performed for each MD subregion to map its whole-brain connectivity patterns. MPMs were generated by assigning each voxel to the corresponding MD subregion with which it showed the greatest number of connections. The numbers in the top row are the coordinates in MNI152 space.

regions. The connection between the MDc and most areas of the orbitofrontal cortex was stronger than the other subregions of the MD. Compared with the other subregions of the MD, the MDd was more strongly connected to the superior prefrontal cortex (medial BA 10), the middle prefrontal cortex (BA 46; lateral BA 10), and the inferior prefrontal cortex (rostral BA 45). The MDl was shown stronger connectivity with the superior prefrontal cortex areas: the medial BA 8, the dorsolateral BA 8, the dorsolateral BA 6, and the medial BA 6; the medial prefrontal cortex areas: the dorsal BA 9/46, the inferior frontal junction, the ventrolateral BA 8, and the ventrolateral BA 6; the inferior prefrontal cortex areas: the dorsal BA 44, the ventral BA 44, and the caudal BA 45; and the caudodorsal BA 24 of the anterior cingulum cortex than the other three parts of the MD.

Overall, there were significant differences in the patterns of connectivity between the MD subregions and the prefrontal regions.

3.3. Functional connectivity patterns of the MD subregions

Detailed whole-brain resting-state functional connectivity seeded from the left and right MD is illustrated in Fig. 4A and Supplementary Fig. S7A, respectively. We observed that the MD subregions had extensive functional connectivity with many brain regions, including the frontal cortex, the cingulate cortex, and the insular cortex. Paired t-tests were used to reveal significant differences in functional connectivity between each pair of MD subregions (please see the up and down triangles in Fig. 4A and Supplementary Fig. S7A). The MDl showed the widest connectivity pattern among the four subregions, and its connectivity with the frontal cortex and occipital cortex are significantly stronger than the MDm and MDc. The connection strength between the MDd and part of the prefrontal lobe is lower than MDl. The MDm is mainly connected with the prefrontal cortex and the precuneus, and the connectivity strength is also significantly smaller than the other three subregions.

We further explore the relationship between the MD subregions and different functional networks, we calculated the common and distinct functional connectivity of the MD subregions with Yeo's seven intrinsic networks (Yeo et al., 2011) and then performed a quantitative comparison. The network connectivity pattern for each MD subregion is displayed in Fig. 4B. The results of the quantitative analysis are shown in Supplementary Table S3. Among the four subregions, the MDm has a strong connection with the high-order cortical networks such as the default network and the frontoparietal network, while the other three

subregions' functional connectivity with the seven networks was relatively evenly distributed. Although the connectivity patterns of the other three sub-regions to the seven functional networks are relatively similar, their connectivity strength showed significant differences. The connectivity strength between the MD subregions and the visual network, the somatomotor network, the ventral attention network, and the dorsal attention network presents an increasing trend from MDm to MDc to MDd to MDl. All the four subregions are significantly connected to the default network and the frontoparietal network, the MDd has the strongest connectivity with the default network. The connectivity between MDd and MDl and the frontoparietal network is significantly stronger than the other two subregions.

The above results all reflect that there is significant connectivity between MD subregions and the prefrontal cortex. A quantitative comparison of the functional connections for the MD subregions was shown in Supplementary Fig. S8 and Table S4. Significantly positive portions of the functional connectivity of the MDl were noted throughout the prefrontal cortex, especially the medial superior prefrontal cortex, the inferior prefrontal cortex, the anterior cingulate cortex, and the insular. The strong connections focused on the middle BA 8 and the middle BA 9 of the medial superior prefrontal cortex. The functional connectivity with the hyper granular insular and rostroventral BA 40 of the inferior parietal lobule was the strongest among the four subregions. While the connectivity of the MDd was overall similar to that of the MDl, the connection strength of the MDl was higher than that of the MDd. Among the four subregions, the functional connectivity strengths of MDm and MDc were lower than the other two subregions. The MDm was mainly connected to the orbital prefrontal cortex, the superior prefrontal cortex, the anterior cingulate cortex, and part of the medial prefrontal cortex. By calculating the correlation between each subregion's structural and functional connectivity patterns on the group level, in particular, we found that the MDm and MDl both had a higher degree of functional and structural coupling compared with the other subregions.

3.4. Relating MD functional connectivity and behaviors

We used PLSC analyses to describe the relationship between each subregion's functional connectivity and various behavioral measures. For each subregion of the MD, one significant LV (MDm LV: 29% of total covariance; singular value = 1.88; $p < 0.05$; MDc LV: 24% of total covariance; singular value = 2.30; $p < 0.05$; MDd LV: 27% of total covariance; singular value = 2.09; $p < 0.05$; MDl LV: 29% of total covari-

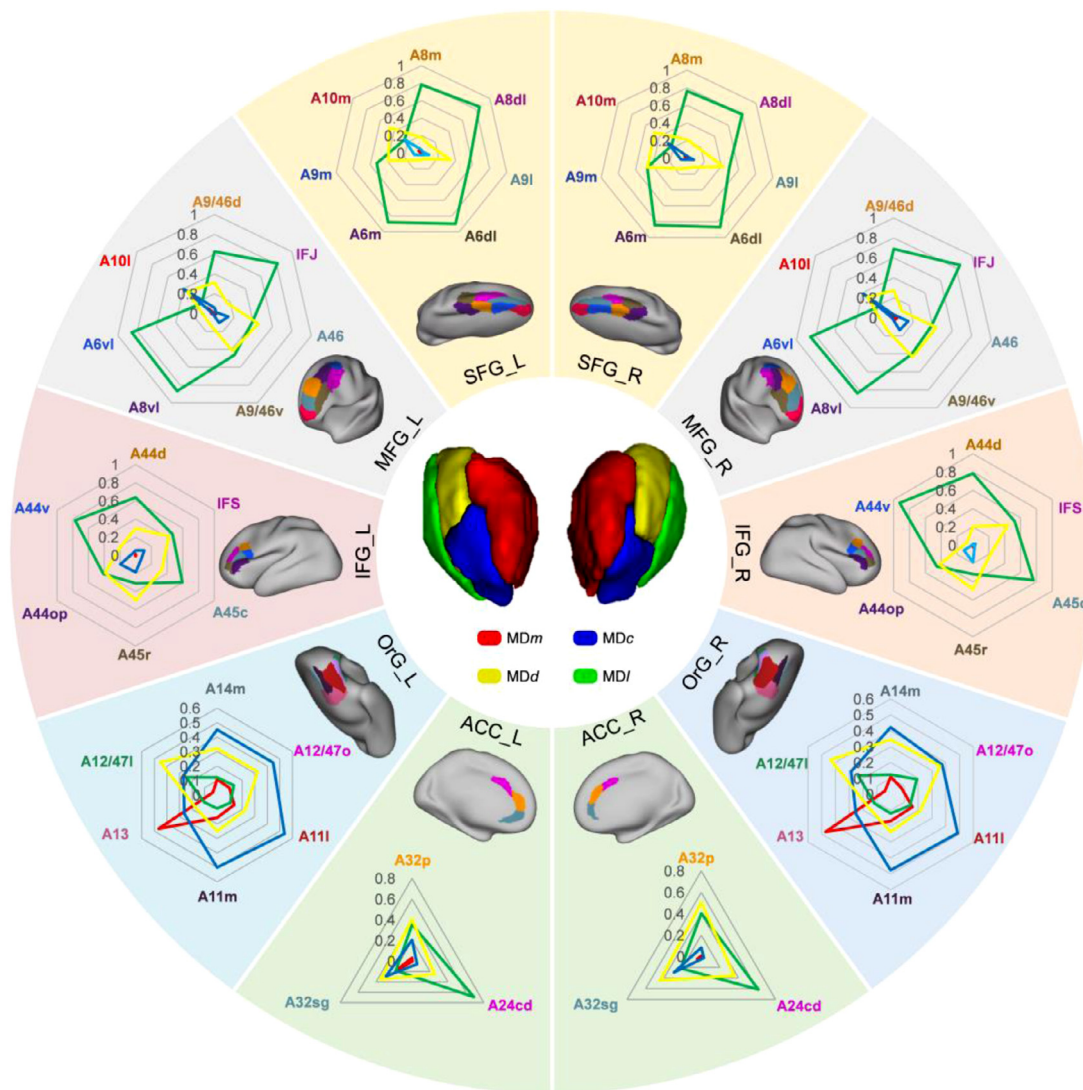


Fig. 3. Connectivity fingerprints of the MD subregions and prefrontal subregions. The left semicircle in the figure shows the connection between the MD subregions of the left hemisphere and the ipsilateral prefrontal area, and the right semicircle showed the same pattern of MD subregions of the right hemisphere. The prefrontal subregions were extracted from the Brainnetome Atlas (Fan et al., 2016). The MDm was mainly connected with the medial orbital frontal cortex, MDc was connected to the lateral orbital cortex, and MDd to the dorsolateral part of the prefrontal cortex. MDl was connected to the dorsomedial and dorsolateral part of the prefrontal cortex. For each target area, the connective differences between the four subregions with each target area were tested using a univariate ANOVA, the results of which are shown in Supplementary Table S2. The prefrontal lobe includes five large regions: SFG (Superior Frontal Gyrus), MFG (Middle Frontal Gyrus), IFG (Inferior Frontal Gyrus), OrG (Orbital Gyrus), ACC (Anterior cingulate cortex), and the vertices of the spider web map in each fan-shaped area correspond to the subregions of these regions.

ance; singular value = 2.62; $p < 0.05$) was identified, a finding which revealed distinct patterns of behavioral measures that map to a single overall set of functional connections.

Virtually all the functional connections of each of the MD subregions with the PFC were found to be reliable through bootstrap resampling, with all the reliable connections loading positively onto their respective LVs (Supplementary Fig. S9). Fig. 5 shows the correlations between the FC of the left MD subregions and behavior, and Supplementary Fig. S10 shows the corresponding results for the right hemisphere. In Fig. 5 the circles show the LV1 correlations between each of the MD subregion's FC and various behaviors. The MD subregion's first LV mainly expressed the behavioral measures of cognition and emotion recognition. The MDc FC-behavior LV showed a close correlation with emotion recognition but had a low correlation with cognition. The MDc FC-behavior LVs MDd FC-behavior LV and MDl FC-behavior LV showed a close correlation with ReactionTimes and ProcSpeed in the cognitive category. However,

the MDd FC-behavior LV and the MDl FC-behavior LV also had a significant correlation with SkippedItems, whereas the MDc FC-behavior LV did not. Inhibition and FluidIntelligence in the cognitive category were only strongly correlated with the MDl FC-behavior LV.

4. Discussion

This study used high-quality DTI data and an advanced connectivity-based parcellation approach to subdivide the human MD into four subregions with distinct anatomical and functional connections. We were also able to characterize the functional consistency and significant functional differences of the different MD subregions from the perspective of their behavioral-functional relationships, indicating that the functional characteristics of brain structure may affect the specific cognitive function and processing needs.

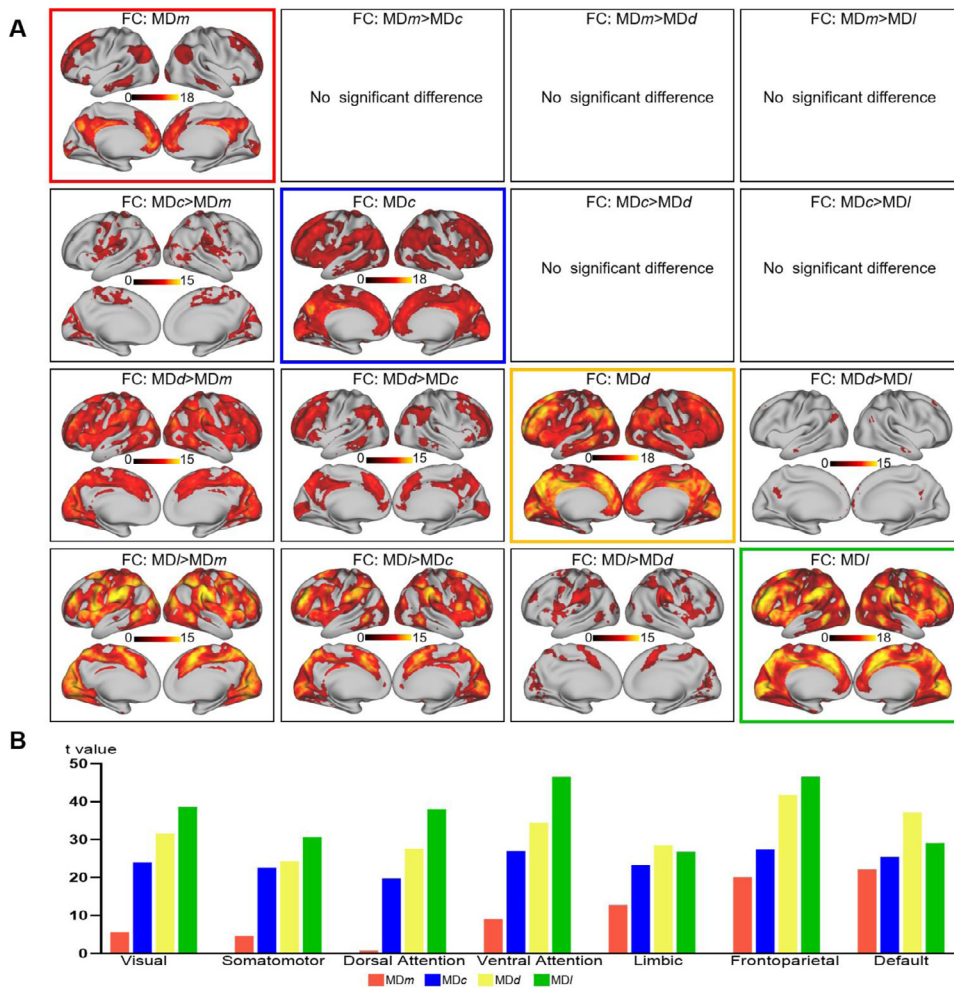


Fig. 4. Resting-state functional connectivity of the left MD subregions. (A) Spatial distribution and paired difference maps of the functional connectivity patterns. The diagonal maps represent the distribution of functional connectivity patterns for each MD subregion. The up and down triangles reveal significant differences in functional connectivity between each pair of MD subregions. For example, MD_d>MD_c represents that in the map the functional connectivity strength of the MD_d is significantly higher than the MD_c. The statistical significance was corrected for family-wise error (FWE) with $p < 0.05$. (B) Functional connectivity patterns between the MD subregions and Yeo's seven intrinsic networks. The connective differences between the four subregions with the seven networks were tested using a univariate ANOVA and a significant result was obtained (Table S3).

4.1. The anatomical organization of the MD subregions

Based on the anatomical connectivity profile with the rest of the human brain, we found that the MD could be robustly subdivided into 4 subregions: medial (MD_m), central (MD_c), dorsal (MD_d), and lateral (MD_l). Previous studies indicated that the MD of adult primates could be subdivided into at least 3 subnuclei based on cytoarchitecture and myeloarchitecture (Mitchell, 2015; Mitchell and Chakraborty, 2013; Pergola et al., 2018). The histological thalamic atlas of Morel et al. (1997) and the Allen human brain reference atlas (Ding et al., 2016) described the histological MD subregions in detail. Allen et al.'s atlas was the first digital human brain atlas to incorporate neuroimaging with high-resolution histology including multiple stains across the entire adult female brain. The densocellular caudodorsal and the parvocellular central (Ding et al., 2016), which are concordant with our MD_c and MD_d. In addition, the magnocellular and multiform divisions of the MD correspond respectively to our MD_m and MD_l subregions. We further performed a parcellation using dMRI data on the same specimen subject as used in Allen et al.'s study and the results were very consistent. The histological map is in line with our parcellations based on in vivo diffusion-weighted imaging and suggests that these subregions differ in both their local histology and connectivity patterns.

Our results revealed distinct anatomy associated with each MD subregion. These maps reflected the topology of the anatomical projections from the MD to the cortex, which follow a particular organization from the MD to the prefrontal cortex (Pergola et al., 2018, 2013). We found that the human MD_m corresponds to the magnocellular medial region and was primarily connected with the medial orbitofrontal cortex and

that the connection of the MD_m with BA 13 was significantly stronger than the other subregions (Klein et al., 2010; Ray and Price, 1993). In some studies, the MD_c and MD_d were treated as unified central regions (Walker, 1940). However, more recent reviews indicated that in primates this area can be further divided into the pars caudodorsalis region and the pars parvocellular rostrocaudal extent of the MD (Abitz et al., 2007; Eckert et al., 2012; Mitchell, 2015; Siwek and Pandya, 1991). The MD_c has a stronger connection with part of the medial frontal cortex and the orbitofrontal cortex, which is also similar to the structural connectivity feature of the pars parvocellular MD (Goldman-Rakic and Porrino, 1985; Xiao et al., 2009). Consistent with our findings, previous studies showed that the MD_d in humans has a strong connection with the anterior cingulate cortex and BA 46, which mainly constitute the dorsolateral prefrontal cortex (Danet et al., 2015; Goldman-Rakic and Porrino, 1985; Klein et al., 2010; Lee and Shin, 2016). The MD_l, which corresponds to the paralaminar or multiform region of the MD strongly connects with the superior and inferior prefrontal cortex and anterior cingulate cortex (Phillips et al., 2019). Since the PFC is mainly associated with executive functions (Ouhaz et al., 2018), our findings may support the concept that the MD is essential to cognition via strong connections with the PFC.

4.2. The functional organization of the MD subregions

Complex tasks depend on signal transmission across multiple brain regions, so the involvement of the MD in different cognitive tasks may depend on the connections between a given MD subregion and other brain regions (Mitchell, 2015; Pergola et al., 2013). To further dissect

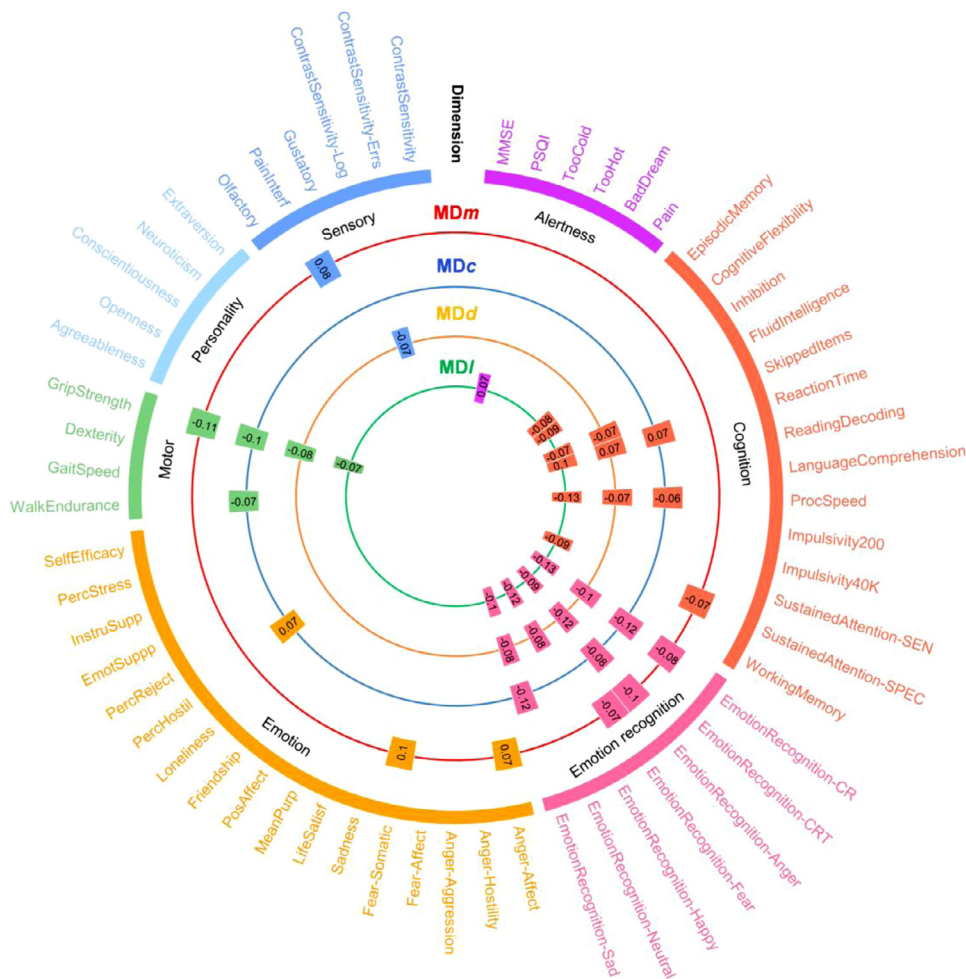


Fig. 5. Correlations between FC and behaviors. The four circles respectively show the behaviors that are significantly associated with each MD subregion in the left hemisphere. The values in the boxes represent the correlation values. Bootstrapping was used to estimate the significance of the brain-behavior correlations.

the cognitive functions of each subregion of the MD, we used PLSC to explore FC-behavior relationships and compared the FC between each MD subregion and the PFC subregions using 59 behavioral measures covering six behavior categories, i.e., cognition, alertness, emotion, motor, personality, and sensory (Izquierdo and Murray, 2010; Metzger et al., 2010). Our result of the FC-behavior relationships showed that each MD subregion captured multiple sets of functional connectivity-behavior associations. We found that each MD subregion had strong functional integration concerning the prefrontal lobe, which is consistent with previous studies, which showed that the role of MD may be related to the maintenance of the prefrontal lobe activity during the cognitive process (Antonucci et al., 2021). From the perspective of different subregions, compared with the MDm, the MDc, MDl, and MDd were involved in multiple cognitive functions. MDd and MDc FC-behavior LVs showed an overlapping set of behaviors with a similar pattern; that is, higher FC between the PFC and MDd/MDc was related to higher fluid intelligence (skipped items, reaction time) and processing speed (ProcSpeed). This suggests that individuals with a higher MDd-PFC or MDc-PFC FC would manifest better performance in these behaviors.

Furthermore, apart from this overlapping set, we observed a unique set of measures, composed of inhibition (Parnaudeau et al., 2013) and cognitive flexibility (CardSort), that were connected with MDl FC-behavior LV, following the pattern that the higher the MDl-PFC FC, the lower the inhibition and cognitive flexibility. Compared with other subregions, the MDl was associated with more behaviors, which seems to have been due to the strong anatomical and functional connections between this brain area and the prefrontal lobe. Unlike the other subregions of the MD, the LV of the MDc captured a variety of MDc connec-

tions to the PFC that contributed positively to the FC-behavior association. These connections showed a positive association with sustained attention, which was the only measure strongly expressed for this association. We also found that all of the MD subregions were associated with the cognitive-emotional (emotion recognition) measure (Tian and Zalesky, 2018). Even the MDm subregion, which showed a mediocre performance in cognition, had a good performance in emotion recognition; this may be due to the main connection between the MDm and the orbital frontal area (Golden et al., 2016). This suggests that, although the MD subregions rely on their functional connections with the PFC to support multiple and overlapping cognitive and cognitive-emotional functions, each of the regions has a more specialized function, which is probably related to differences in their FC strengths. Future studies using task fMRI data or clinical data may further investigate these results from other perspectives.

4.3. Limitations

Previous studies have shown that the volume of MD changes during aging (Fama and Sullivan, 2015; Rosenberg et al., 2016), the research on MD at different ages is also a very meaningful issue. In this study, we conducted in-depth explorations on the sub-regions of MD and their anatomical and functional connections in a group of healthy adults, which provided a complete methodological reference for the subsequent research on MD at different ages. We look forward to systematic research in future work.

HCP rs-fMRI data has high a spatial and temporal resolution, however, it is known that the signal-to-noise ratio of its subcortex is low.

We have taken several means to improve the quality of the data as the previous research on subcortical regions (Ely et al., 2019; Guedj and Vuilleumier, 2020). We performed low-pass filtering on the minimally preprocessed data to kick out the uninterested physiological signals. Although a part of the high-frequency signal was lost, the signal-to-noise ratio of the subcortex data was improved. Due to the small size of MD, to avoid signal confusion between the sub-regions and reduce the impact of low resolution, the MD region was not smoothed. In addition to the issues of resolution and filtering, we also considered the issues of signal-to-noise ratio and size. There is no significant difference in the signal-to-noise ratio of the four sub-regions, and the volume sizes are relatively consistent. We describe associations between behavioral measures and the functional connectivity of each MD subregion. While these findings indicate a relationship between the intrinsic organization of the MD subregion and behavioral measures, the correlation values are small. Although we have used high-resolution resting-state MRI data, since the MD subregions are relatively small and there are overlaps behaviors that are related to different subregions. We hope to use higher resolution data for further research in the future.

5. Conclusions

In this study, we identified the connectivity-based organization of the human MD and discovered the similarity and specificity of each subregion in terms of its anatomical and functional connectivity. In addition, we explored the relationship between the functional connection of each subregion and behavioral measures, which revealed the role of different subregions in cognition. The findings provide convincing support for further research on the MD. For example, deep brain stimulation applied to MD has been repeatedly reported in animal models, but it has rarely been studied in humans (Mavridis, 2014); our precise subdivisions of the MD will provide evidence for the application of DBS in humans. Moreover, we will investigate cross-species comparisons to further understand the evolution and function of the MD and explore the role of the MD in neuropsychiatric disorders.

Findings

The HCP data that support the findings of this study are publicly available on the Connectome DB database (<https://db.humanconnectome.org>). The code is available from the authors upon request.

Declaration of competing interests

The authors declare no competing interests.

Credit authorship contribution statement

Kaixin Li: Formal analysis, Writing – original draft. **Lingzhong Fan:** Formal analysis, Writing – original draft, Funding acquisition. **Yue Cui:** Writing – original draft, Funding acquisition. **Xuehu Wei:** Writing – original draft. **Yini He:** Writing – original draft. **Jiyue Yang:** Writing – original draft. **Yuheng Lu:** Writing – original draft. **Wen Li:** Writing – original draft. **Weiyang Shi:** Writing – original draft. **Long Cao:** Writing – original draft. **Luqi Cheng:** Writing – original draft. **Ang Li:** Writing – original draft. **Bo You:** Writing – original draft, Project administration, Supervision. **Tianzi Jiang:** Conceptualization, Funding acquisition, Project administration, Supervision, Validation, Writing – review & editing.

Acknowledgments

This work was partially supported by the **National Natural Science Foundation of China** (Grant Nos. 91432302, 31620103905, 82072099 and 31771076), the Science Frontier Program of the Chinese Academy

of Sciences (Grant No. QYZDJ-SSW-SMC019), Beijing Municipal Science and Technology Commission (Grant Nos. Z161100000216139, Z171100000117002), Beijing Advanced Discipline Fund, the Guangdong Pearl River Talents Plan (2016ZT06S220). Data were provided by the Human Connectome Project, WU-Minn Consortium (Principal Investigators: David Van Essen and Kamil Ugurbil; 1U54MH091657) funded by the 16 NIH Institutes and Centers that support the NIH Blueprint for Neuroscience Research; and by the McDonnell Center for Systems Neuroscience at Washington University. The authors declare that the research was conducted in the absence of any commercial or financial relationships that could be construed as a potential conflict of interest. We thank Rhoda E. and Edmund F. Perozzi, PhDs, for English language and editing assistance.

Supplementary materials

Supplementary material associated with this article can be found, in the online version, at doi:10.1016/j.neuroimage.2022.118876.

References

- Abitz, M., Nielsen, R.D., Jones, E.G., Laursen, H., Graem, N., Pakkenberg, B., 2007. Excess of neurons in the human newborn mediodorsal thalamus compared with that of the adult. *Cereb. Cortex* 17, 2573–2578.
- Alelí-Paz, R., Giménez-Amaya, J.M., 2008. The mediodorsal thalamic nucleus and schizophrenia. *J. Psych. Neurosci.* 33, 489.
- Antonucci, L.A., Penzel, N., Pigoni, A., Dominke, C., Kambeitz, J., Pergola, G., 2021. Flexible and specific contributions of thalamic subdivisions to human cognition. *Neurosci. Biobehav. Rev.*
- Baldassano, C., Beck, D.M., Fei-Fei, L., 2015. Parcellating connectivity in spatial maps. *PeerJ* 3, e784.
- Behrens, T.E., Berg, H.J., Jbabdi, S., Rushworth, M.F., Woolrich, M.W., 2007. Probabilistic diffusion tractography with multiple fibre orientations: what can we gain? *Neuroimage* 34, 144–155.
- Byne, W., Buchsbaum, M.S., Mattiace, L.A., Hazlett, E.A., Kemether, E., Elhakem, S.L., Purohit, D.P., Haroutunian, V., Jones, L., 2002. Postmortem assessment of thalamic nuclear volumes in subjects with schizophrenia. *Am. J. Psychiatry* 159, 59–65.
- Calamante, F., Tournier, J.-D., Jackson, G.D., Connelly, A., 2010. Track-density imaging (TDI): super-resolution white matter imaging using whole-brain track-density mapping. *Neuroimage* 53, 1233–1243.
- Caspers, S., Eickhoff, S.B., Geyer, S., Scheperjans, F., Mohlberg, H., Zilles, K., Amunts, K., 2008. The human inferior parietal lobule in stereotaxic space. *Brain Struct. Funct.* 212, 481–495.
- Cheng, C., Fan, L., Xia, X., Eickhoff, S.B., Li, H., Li, H., Chen, J., Jiang, T., 2018. Rostro-caudal organization of the human posterior superior temporal sulcus revealed by connectivity profiles. *Hum Brain Mapp* 39, 5112–5125.
- Cheng, L., Zhang, Y., Li, G., Wang, J., Sherwood, C., Gong, G., Fan, L., Jiang, T., 2021. Connectional asymmetry of the inferior parietal lobule shapes hemispheric specialization in humans, chimpanzees, and rhesus macaques. *Elife* 10, e67600.
- Danet, L., Barbeau, E.J., Eustache, P., Planton, M., Raposo, N., Sibon, I., Albucher, J.-F., Bonneville, F., Peran, P., Pariente, J., 2015. Thalamic amnesia after infarct: the role of the mammillothalamic tract and mediodorsal nucleus. *Neurology* 85, 2107–2115.
- Ding, S.-L., Royall, J.J., Sunkin, S.M., Ng, L., Facer, B.A.C., Lesnar, P., Guillozet-Bongaarts, A., McMurray, B., Szafer, A., Dolbeare, T.A., Stevens, A., Tirrell, L., Benner, T., Caldejon, S., Dalley, R.A., Dee, N., Lau, C., Nyhus, J., Reding, M., Riley, Z.L., Sandman, D., Shen, E., van der Kouwe, A., Varjabedian, A., Write, M., Zollei, L., Dang, C., Knowles, J.A., Koch, C., Phillips, J.W., Sestan, N., Wahnoutka, P., Zielke, H.R., Hohmann, J.G., Jones, A.R., Bernard, A., Hawrylycz, M.J., Hof, P.R., Fischl, B., Lein, E.S., 2016. Comprehensive cellular-resolution atlas of the adult human brain. *J. Comp. Neurol.* 524, 3127–3481.
- Eckert, U., Metzger, C.D., Buchmann, J.E., Kaufmann, J., Osoba, A., Li, M., Safron, A., Liao, W., Steiner, J., Bogerts, B., 2012. Preferential networks of the mediodorsal nucleus and centromedian-parafascicular complex of the thalamus—A DTI tractography study. *Hum Brain Mapp* 33, 2627–2637.
- Ely, B.A., Stern, E.R., Kim, J.-w., Gabbay, V., Xu, J., 2019. Detailed mapping of human habenula resting-state functional connectivity. *Neuroimage*.
- Fama, R., Sullivan, E.V., 2015. Thalamic structures and associated cognitive functions: relations with age and aging. *Neurosci. Biobehav. Rev.* 54, 29–37.
- Fan, L., Li, H., Zhuo, J., Zhang, Y., Wang, J., Chen, L., Yang, Z., Chu, C., Xie, S., Laird, A.R., 2016. The human brainnetome atlas: a new brain atlas based on connective architecture. *Cereb. Cortex* 26, 3508–3526.
- Fan, X., Thompson, M., Bogovic, J.A., Bazin, P.-L., Prince, J.L., 2011. A novel contrast for DTI visualization for thalamus delineation. *Medical Imaging 2010: Visualization, Image-Guided Procedures, and Modeling*. International Society for Optics and Photonics.
- Georgescu, I.A., Popa, D., Zagrean, L., 2020. The anatomical and functional heterogeneity of the mediodorsal thalamus. *Brain Sci.* 10, 624.
- Glasser, M.F., Sotiropoulos, S.N., Wilson, J.A., Coalson, T.S., Fischl, B., Andersson, J.L., Xu, J., Jbabdi, S., Webster, M., Polimeni, J.R., 2013. The minimal preprocessing pipelines for the Human Connectome Project. *Neuroimage* 80, 105–124.

- Golden, E.C., Graff-Radford, J., Jones, D.T., Benarroch, E.E., 2016. Mediodorsal nucleus and its multiple cognitive functions. *Neurology* 87, 2161–2168.
- Goldman-Rakic, P.S., Porrino, L.J., 1985. The primate mediodorsal (MD) nucleus and its projection to the frontal lobe. *J. Comp. Neurol.* 242, 535–560.
- Guedj, C., Vuilleumier, P., 2020. Functional connectivity fingerprints of the human pulvinar: decoding its role in cognition. *Neuroimage* 221, 117162.
- Guillery, R., 1995. Anatomical evidence concerning the role of the thalamus in cortico-cortical communication: a brief review. *J. Anat.* 187, 583.
- Haber, M., McFarland, N.R., 2001. The place of the thalamus in frontal cortical-basal ganglia circuits. *Neuroscientist* 7, 315–324.
- Izquierdo, A., Murray, E.A., 2010. Functional interaction of medial mediodorsal thalamic nucleus but not nucleus accumbens with amygdala and orbital prefrontal cortex is essential for adaptive response selection after reinforcer devaluation. *J. Neurosci.* 30, 661–669.
- Johansen-Berg, H., Behrens, T., Robson, M., Drobznjak, I., Rushworth, M., Brady, J., Smith, S., Higham, D., Matthews, P., 2004. Changes in connectivity profiles define functionally distinct regions in human medial frontal cortex. *Proc. Natl. Acad. Sci.* 101, 13335–13340.
- Jones, E.G., 2012. *The Thalamus*. Springer Science & Business Media.
- Klein, J.C., Rushworth, M.F., Behrens, T.E., Mackay, C.E., de Crespigny, A.J., D'Arceuil, H., Johansen-Berg, H., 2010. Topography of connections between human prefrontal cortex and mediodorsal thalamus studied with diffusion tractography. *Neuroimage* 51, 555–564.
- Lee, S., Shin, H.-S., 2016. The role of mediodorsal thalamic nucleus in fear extinction. *J. Anal. Sci. Technol.* 7, 1–5.
- Liu, Y., D'Haese, P.-F., Newton, A.T., Dawant, B.M., 2020. Generation of human thalamus atlases from 7 T data and application to intrathalamic nuclei segmentation in clinical 3 T T1-weighted images. *Magn Reson Imaging* 65, 114–128.
- Marcus, D., Harwell, J., Olsen, T., Hodge, M., Glasser, M., Prior, F., Jenkinson, M., Laumann, T., Curtiss, S., Van Essen, D., 2011. Informatics and data mining tools and strategies for the human connectome project. *Front. Neuroinform.* 5, 4.
- Mavridis, I., 2014. Human mediodorsal thalamic nucleus as a potential target for deep brain stimulation: review of the literature and anatomical considerations. *OA Anat.* 2, 1.
- McIntosh, A.R., Bookstein, F.L., Haxby, J.V., Grady, C.L., 1996. Spatial pattern analysis of functional brain images using partial least squares. *Neuroimage* 3, 143–157.
- McIntosh, A.R., Lobaugh, N.J., 2004. Partial least squares analysis of neuroimaging data: applications and advances. *Neuroimage* 23, S250–S263.
- Metzger, C.D., Eckert, U., Steiner, J., Sartorius, A., Buchmann, J.E., Stadler, J., Tempelmann, C., Speck, O., Bogerts, B., Abler, B., 2010. High field fMRI reveals thalamo-cortical integration of segregated cognitive and emotional processing in mediodorsal and intralaminar thalamic nuclei. *Front. Neuroanat.* 4, 138.
- Mišić, B., Betzel, R.F., De Reus, M.A., Van Den Heuvel, M.P., Berman, M.G., McIntosh, A.R., Sporns, O., 2016. Network-level structure-function relationships in human neocortex. *Cereb. Cortex* 26, 3285–3296.
- Mitchell, A.S., 2015. The mediodorsal thalamus as a higher order thalamic relay nucleus important for learning and decision-making. *Neurosci. Biobehav. Rev.* 54, 76–88.
- Mitchell, A.S., Browning, P.G., Baxter, M.G., 2007. Neurotoxic lesions of the medial mediodorsal nucleus of the thalamus disrupt reinforcer devaluation effects in rhesus monkeys. *J. Neurosci.* 27, 11289–11295.
- Mitchell, A.S., Chakraborty, S., 2013. What does the mediodorsal thalamus do? *Front. Syst. Neurosci.* 7, 37.
- Morel, A., Magnin, M., Jeanmonod, D., 1997. Multiarchitectonic and stereotactic atlas of the human thalamus. *J. Comp. Neurol.* 387, 588–630.
- Ouhaz, Z., Fleming, H., Mitchell, A.S., 2018. Cognitive functions and neurodevelopmental disorders involving the prefrontal cortex and mediodorsal thalamus. *Front. Neurosci.* 12, 33.
- Oyoshi, T., Nishijo, H., Asakura, T., Takamura, Y., Ono, T., 1996. Emotional and behavioral correlates of mediodorsal thalamic neurons during associative learning in rats. *J. Neurosci.* 16, 5812–5829.
- Pergola, G., Danet, L., Pitel, A.-L., Carlesimo, G.A., Segobin, S., Pariente, J., Suchan, B., Mitchell, A.S., Barbeau, E.J., 2018. The regulatory role of the human mediodorsal thalamus. *Trends Cogn. Sci. (Regul. Ed.)* 22, 1011–1025.
- Pergola, G., Ranft, A., Mathias, K., Suchan, B., 2013. The role of the thalamic nuclei in recognition memory accompanied by recall during encoding and retrieval: an fMRI study. *Neuroimage* 74, 195–208.
- Phillips, J.M., Fish, L.R., Kambi, N.A., Redinbaugh, M.J., Mohanta, S., Kecskemeti, S.R., Saalman, Y.B., 2019. Topographic organization of connections between prefrontal cortex and mediodorsal thalamus: evidence for a general principle of indirect thalamic pathways between directly connected cortical areas. *Neuroimage* 189, 832–846.
- Ray, J.P., Price, J.L., 1992. The organization of the thalamocortical connections of the mediodorsal thalamic nucleus in the rat, related to the ventral forebrain-prefrontal cortex topography. *J. Comp. Neurol.* 323, 167–197.
- Ray, J.P., Price, J.L., 1993. The organization of projections from the mediodorsal nucleus of the thalamus to orbital and medial prefrontal cortex in macaque monkeys. *J. Comp. Neurol.* 337, 1–31.
- Rosenberg, M.D., Finn, E.S., Scheinost, D., Papademetris, X., Shen, X., Constable, R.T., Chun, M.M., 2016. A neuromarker of sustained attention from whole-brain functional connectivity. *Nat. Neurosci.* 19, 165–171.
- Sherman, S.M., 2007. The thalamus is more than just a relay. *Curr. Opin. Neurobiol.* 17, 417–422.
- Siwek, D.F., Pandya, D.N., 1991. Prefrontal projections to the mediodorsal nucleus of the thalamus in the rhesus monkey. *J. Comp. Neurol.* 312, 509–524.
- Su, J.H., Thomas, F.T., Kasoff, W.S., Tournias, T., Choi, E.Y., Rutt, B.K., Saranathan, M., 2019. Thalamus optimized multi atlas segmentation (THOMAS): fast, fully automated segmentation of thalamic nuclei from structural MRI. *Neuroimage* 194, 272–282.
- Tian, Y., Zalesky, A., 2018. Characterizing the functional connectivity diversity of the insula cortex: subregions, diversity curves and behavior. *Neuroimage* 183, 716–733.
- Tungaraza, R.L., Mehta, S.H., Haynor, D.R., Grabowski, T.J., 2015. Anatomically informed metrics for connectivity-based cortical parcellation from diffusion MRI. *IEEE J. Biomed. Health Inform.* 19, 1375–1383.
- Van Essen, D.C., Smith, S.M., Barch, D.M., Behrens, T.E., Yacoub, E., Ugurbil, K., Consortium, W.-M.H., 2013. The WU-Minn human connectome project: an overview. *Neuroimage* 80, 62–79.
- Victor, M., 1989. The Wernicke-Korsakoff syndrome and related neurologic disorders due to alcoholism and malnutrition. *Contemp. Neurol. Ser.* 30.
- Walker, A.E., 1940. The medial thalamic nucleus. A comparative anatomical, physiological and clinical study of the nucleus medialis dorsalis thalami. *J. Comp. Neurol.* 73, 87–115.
- Xia, X., Fan, L., Cheng, C., Eickhoff, S.B., Chen, J., Li, H., Jiang, T., 2017. Multimodal connectivity-based parcellation reveals a shell-core dichotomy of the human nucleus accumbens. *Hum. Brain Mapp.* 38, 3878–3898.
- Xiao, D., Zikopoulos, B., Barbas, H., 2009. Laminar and modular organization of prefrontal projections to multiple thalamic nuclei. *Neuroscience* 161, 1067–1081.
- Yeo, B.T., Krienen, F.M., Sepulcre, J., Sabuncu, M.R., Lashkari, D., Hollinshead, M., Roffman, J.L., Smoller, J.W., Zöllei, L., Polimeni, J.R., 2011. The organization of the human cerebral cortex estimated by intrinsic functional connectivity. *J. Neurophysiol.*
- Zhang, Y., Larcher, K.M.-H., Mistic, B., Dagher, A., 2017. Anatomical and functional organization of the human substantia nigra and its connections. *Elife* 6, e26653.
- Zhuo, J., Fan, L., Liu, Y., Zhang, Y., Yu, C., Jiang, T., 2016. Connectivity profiles reveal a transition subarea in the parahippocampal region that integrates the anterior temporal-posterior medial systems. *J. Neurosci.* 36, 2782–2795.
- Zimmermann, J., Griffiths, J.D., McIntosh, A.R., 2018. Unique mapping of structural and functional connectivity on cognition. *J. Neurosci.* 38, 9658–9667.